MTT-22, pp. 486–493, May 1974.
[3] J. A. Arnaud and F. A. Pelow, "Resonant grid quasi-optical diplexers," *Bell Syst. Tech. J.*, vol. 54, no. 2, pp. 263–283, 1975.
[4] C. C. Chen, "Transmission of microwaves through perforated flat plates of finite thickness," *IEEE Trans. Microwave Theory Tech.*, vol. MTT-21, pp. 1–6, Jan. 1973.
[5] R. J. Luebbers and B. A. Munk, "Some effects of dielectric loading on periodic slot arrays," *IEEE Trans. Antennas Propagat.*, vol. AP-26, pp. 536–542, Apr. 1978.
[6] N. Ammitay, V. Galindo, and C. P. Wu, *Theory and Analysis of Phased Array Antennas*. New York: Wiley, 1972.
[7] J. J. Fratamico, "A wide scan quasi-optical frequency diplexer," S.M. thesis, Massachusetts Institute of Technology, Cambridge, MA, 1980.
[8] J. F. Carlson and A. Heins, "The reflection of an electromagnetic plane wave by an infinite set of plates," *Quart. Appl. Math.*, 4, no. 4, pp. 313–329, 1947.
[9] P. D. Potter, "A new horn antenna with suppressed sidelobes and equal beamwidths," *Microwave J.*, vol. 6, pp. 71–78, 1963.

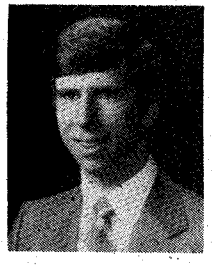

John J. Fratamico, Jr. was born in Glens Falls, NY on March 6, 1957. He received the S.B., S.M., and Eng. degrees in electrical engineering in 1980, 1980, and 1981, respectively, all from the Massachusetts Institute of Technology, Cambridge.

He is presently working toward his doctorate at M.I.T., with fellowship support from the Fannie and John Hertz Foundation. His current research interests include the design of curved dichroic surfaces, and the propagation of millimeter waves through a turbid atmosphere.

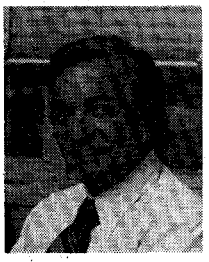

Michael J. Gans received the B.S. degree in electrical engineering from Notre Dame University, South Bend, IN, in 1957, and the M.S. and Ph.D. degrees in electrical engineering from the University of California, Berkeley, in 1961 and 1965, respectively.

At Bell Laboratories, he has been engaged in research on antennas for mobile radio and satellite communications.

Gerald J. Owens served in the U.S. Navy from 1950 to 1954. He joined Bell Laboratories, Holmdel, NJ, in 1955. He was associated with various military radar projects, the earth station tracking receivers for the Telstar project, solar radio telescopes, and, more recently, computer controlled voice response systems. He is currently engaged in research on satellite antennas.

Numerical Evaluation of Lumped Inductance Influences of Superconducting Circuit Interconnections on Ultrafast Switching Signal Propagation Characteristics

JIRO TEMMYO AND HARUO YOSHIKIYO

Abstract—**The lumped inductance influences of superconducting circuit interconnections on ultrafast switching (~10 ps) signal propagation characteristics, such as propagation delay, degraded switching time, reflections, amplitude distortions, and crosstalk, were for the first time quantitavely evaluated by using the LNAP computer simulation, including the influences of matching capacitors and terminated resistor value.**

Manuscript received February 27, 1981; revised August 18, 1981.

The authors are with the Musashino Electrical Communication Laboratory, Nippon Telegraph and Telephone Public Corporation, 3-9-11, Midoricho, Musashino-shi, 180 Tokyo, Japan.

I. INTRODUCTION

JOSEPHSON LOGIC and memory chips are being investigated to evaluate its potential for high performance computers [1]. The very low power dissipation of Josephson chips permits its high circuit density per unit

0018-9480/82/0001-0027$00.75 ©1982 IEEE

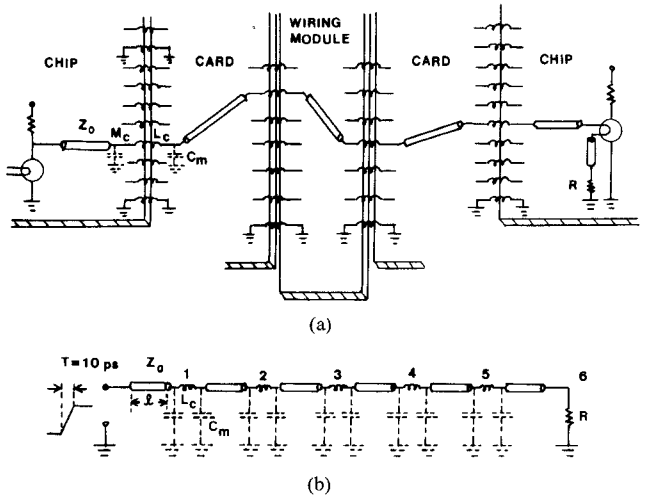

Fig. 1. Superconducting transmission line. (a) Circuit configuration. (b) Schematic circuit for computer simulation.

volume without creating heat removal problems [1]. Moreover, all the on-chip and off-chip signals in the Josephson technology are transmitted using matched lossless superconducting transmission lines over a superconducting groundplane. To take full advantages of the ultrafast switching speeds (~10 ps) [2] of the junction circuits, the physical distances between various units of a system and the resulting signal propagation delays become very significant and must be as small as possible.

Brown has shown an overall packaging philosophy for high speed Josephson computers in detail [3]. Jones *et al.* have reported the characteristics of chip-to-chip signal propagation in a package suitable for superconducting circuits [4]. Lahiri *et al.* have also reported the miniaturized pluggable connectors for Josephson device packaging in order to increase the circuit density and reduce the package interconnection delay [5]. Moreover, recently, an ultrahigh resolution Josephson technology sampling system has been designed and successfully tested, resulting in measuring complex test signals containing a 10-ps rise time directly [6],[7].

However, to the authors' knowledge, the lumped inductance influences of superconducting circuit interconnections, which inevitably exist in ultrafast switching signal propagation characteristics, such as propagation delay, degraded switching time, reflections, amplitude distortions, and crosstalk, have not been clarified in detail.

The purpose of this paper is mainly to determine the fundamental quantitative relation between the lumped (self and mutual) inductances and various distorted electrical properties in order to design and realize high performance switching equipment. First, in the time domain, the influences of the lumped interconnection inductances, which inevitably appear at various discontinuities, were clarified by computer simulation using the LNAP program [8]. For the circuits, as shown in Fig. 1, including interconnection inductances between Josephson chip-to-card, card-to-wiring module, and lumped inductance at the Josephson gate, propagation delay, reflection amplitude, amplitude distortion, and rise time changes at the discontinuities are estimated, including the matched capacitor effect and the termination resistor effect, so that one can determine the allowable interconnection inductance values if the high machine performance values are given.

Section II mainly covers the computer simulation results for the circuit as shown in Fig. 1, including considerations in the frequency domain. Section III describes some considerations on Josephson interconnections. Section IV gives summary and conclusions.

II. Circuit Simulation

A. Basic Considerations

Let us consider the circuit configuration as shown in Fig. 1. Here it is assumed that the Josephson chips, cards, and wiring module are all made up of lossless superconducting striplines, whose characteristic impedance is $Z_0 = 10\ \Omega$. At the various inductive discontinuities, superconducting contacts are assumed to be available and self- and mutual inductances at the discontinuities are written as L_c and M_c, respectively. Matching capacitors are shown as C_m. In order to make clear the electrical properties at the inductive discontinuities, the Josephson gate is approximated as a ramped input voltage positive-going source wave, and its rise time t_r (10–90 percent) is assumed as 8 ps. Before making the computer simulation in the time domain, the frequency bandwidth of the input ramped voltage source must be considered in the frequency domain. Fig. 2 (a) shows the Fourier spectrum for the input signal $f(t)$ shown in Fig. 2 (a) with $T = 10$ ps and given as follows:

$$F(\omega) = \pi\delta(\omega) - j\frac{2\sin\left(\frac{\omega T}{2}\right)}{T\omega^2} \tag{1}$$

$$\omega = 2\pi f \tag{2}$$

where f is the frequency and $\delta(\omega)$ is Dirac's delta function. Above the frequency of about 400 GHz, the spectrum amplitudes are small enough to be ignored. On the other hand, in order to analyze the stripline using the LNAP program, the striplines must be approximated by the chains of the LC ladder circuits. The LC π-filter circuit shown in Fig. 2 (b) shows the low-pass filtering performance with the cutoff frequency (3 dB down) f_c, which is given by

$$f_c = \frac{1}{\pi\sqrt{LC}}. \tag{3}$$

Accordingly, the lumped L and C values for the ladder circuit must be chosen so that the f_c value is high enough compared with the input signal bandwidth. For example, an Nb superconducting stripline with $Z_0 = 10\ \Omega$ is assumed, where linewidth $w = 10\ \mu$m. Other assumptions are SiO insulation layer whose thickness $h_{SiO} = 0.4\ \mu$m, lumped inductance L_0 and capacitance C_0 values per 100-μm length of 7.5 pH/100 μm and 0.075 pF/100 μm, respectively, resulting in the cutoff frequency $f_c^0 = 424$ GHz. In Fig. 2 (b), for $L = L_0$ and $C = C_0$, the calculated amplitude and phase frequency responses are shown as line 1. On the other hand, the propagation delay τ_π at one LC filter is

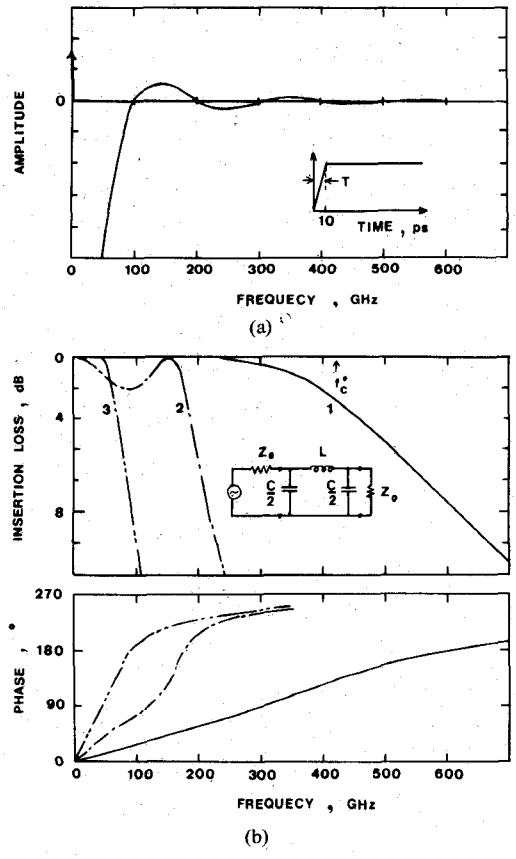

Fig. 2. Ramp input voltage waveform $f(t)$. (a) Its Fourier Spectrum $F(\omega)=\pi\delta(\omega)-j(2\sin(\omega T/2)/T\omega^2)$, $\omega=2\pi f$. (b) LC π-filter for consideration and its frequency responses. Line 1: $L=L_0=7.5$ pH; $C=C_0=0.075$ pF. Line 2: $L=L_c=50$ pH; $C=C_0$. Line 3: $L=L_c$; $C=0.5$ pF.

given by

$$\tau_\pi=\sqrt{LC}. \tag{4}$$

Accordingly, for $L=L_0$ and $C=C_0$, the propagation delay per 100-μm length is 0.075 ps/100 μm and so 7.5 ps/1 mm.

B. Interconnection Self-Inductance Influences

In Fig. 2 (b), for $L=L_c>L_0$, the matching capacitor C_m is given by

$$C_m=\frac{1}{2}C=\frac{L_c}{2Z_0^2}. \tag{5}$$

For example, in Fig. 2 (b), for both cases of $L=L_c=50$ pH and $C=C=0.075$ pF and/or $C=C_m=0.25$ pF (matched case), the calculated frequency responses are shown by line 2 and line 3, respectively. For the unmatched case, the frequency response does not show perfect low-pass performance, but 2-dB loss is observed near 80 GHz, and the cutoff frequency f_c (3 dB down) is about 180 GHz, which is 165 GHz provided (3) is used simply. For the matched case, perfect low-pass filter performance is obtained with cutoff frequency $f_c=65$ GHz, resulting in the large limitation of the passband. Fig. 3 shows relations between lumped interconnection inductances and matching capacitor values and/or cutoff frequencies, with Z_0 as parameters. For the case where the interconnection inductance exhibits some constant value, the characteristic impedance Z_0 is smaller, distortions observed become smaller and, moreover, the matched capacitor and cutoff frequency values needed become smaller.

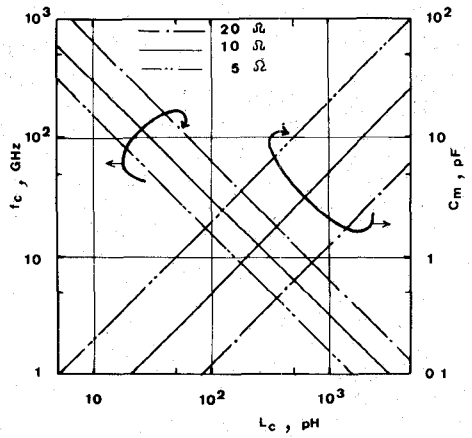

Fig. 3. Relation between lumped inductance L_c and matching capacitance C_m and/or cutoff frequency f_c.

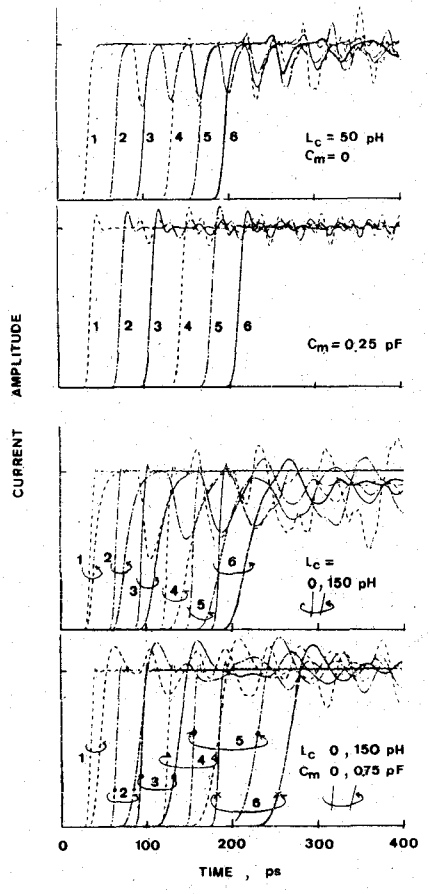

Fig. 4. Current waveforms for the circuit shown in Fig. 1 (b) without and/or with matching capacitors C_m. (a) $L_c=50$ pH. (b) $L_c=150$ pH.

The time domain responses for the circuit shown in Fig. 1 (b), are shown in Fig. 4 (a) and (b) using the LNAP program. Here, the characteristic impedance Z_0 is 10 Ω constant, all the lossless superconducting stripline lengths are $l=4$ mm constant, which is near the worst case from the electrical distortion standpoint, the lumped inductance

L_c values are 50 pH constant in Fig. 4 (a) and 150 pH constant in Fig. 4 (b), respectively, mutual inductances at the discontinuities are ignored here and the end resistor R of the line is terminated into characteristic impedance Z_0 for the line. The traces of No.1–6 in Fig. 4 (a) and (b) for both cases of without and/or with matching capacitors at the inductive discontinuities No. 1–5 in Fig. 1 (b) are the current waveforms. In particular, in Fig. 4 (b), the current waveforms of No. 1 to No. 6 for the case of $L_c=0$ are also shown, in order to clarify the inductive discontinuity effects.

Some features of these current waveforms without matching capacitors are as follows: the negative pulse-like reflections occur so that a ripple with $2\tau_{4\ mm}=60$-ps period, which is the round-trip time for the stripline, is observed. For example, at about 100 ps, a "dip" of -0.40 relative amplitude is observed in trace 1 without matching capacitors in Fig. 4 (a), which is caused by the reflections at both No. 1 and No. 2 inductive discontinuities. On the other hand, the current at the matched terminated resistor shows ripple which is decreased by the influence of the existence of re-reflections and mismatches in the reflection wave phases. Signal rise times are degraded gradually after passing through the inductive discontinuities, because of the influences of the large limitation of the passing signal bandwidth.

Next, for the matched case, the reflections at the discontinuities are eliminated completely. However, the ± 10-percent amplitude vibrations at the stationary current value occur because of the influences of the decreased cutoff frequency f_c. The rising performance of the signal exhibits overshoot tendency, resulting in an improved rise time, compared with the unmatched case. However, propagation delays at the inductive discontinuities with matching capacitors are increased, but the shape of the pulse is relatively maintained. Increasing the lumped inductances without matching capacitors causes a degradation of the switching time for the forward-going wave, as it passes through the inductive discontinuity, and an increase in propagation delay and signal reflection, while, for the matching case, the reflection is eliminated completely and amplitude vibration is largely observed in the stationary values. Concerning the propagation delay, compared with the $L_c=0$ case, the current at the terminated resistor is typically delayed by 75 ps.

Relations between lumped inductance L_c versus propagation delay, degradated switching time, and current reflection coefficient r_I can be are summarized as follows: Fig. 5 shows the relation between calculated propagation delay and the lumped inductance, including the effect of matching capacitors. Circular and rectangular signs indicate the simulation results, and lines 1 and 2 show calculated values using (4) for the matching capacitors. The dashed line shows the calculated value for $Z_0=5\ \Omega$ with matching capacitors at the inductive discontinuity. For example, at a typical case of $L_c=200$ pH with matching capacitors of 1 pF, a propagation delay of 20 ps occurs at this discontinuity, which equals, for example, the propagation delay for

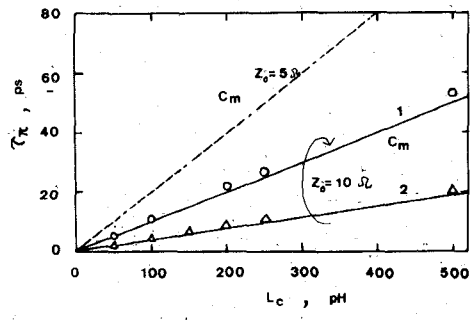

Fig. 5. Relation between propagation delay at discontinuity and lumped inductance L_c.

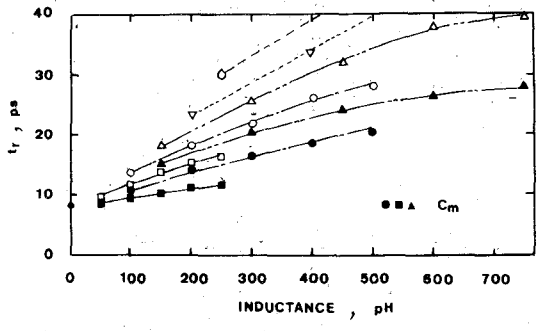

Fig. 6. Relation between signal rise time t_r and summed inductance value at each discontinuity.

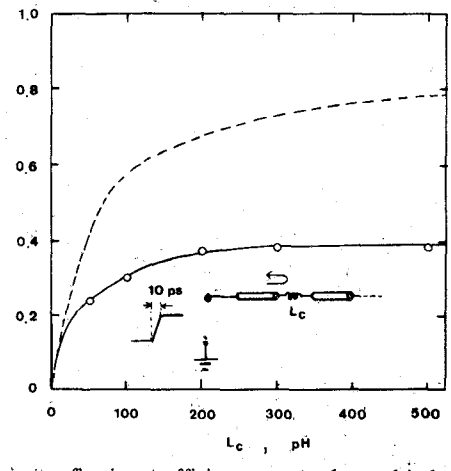

Fig. 7. Current reflection coefficient r_I versus lumped inductance value L_c at discontinuity.

the 2.4-mm line with $Z_0=10\ \Omega$. It is also found that, as characteristic impedance becomes smaller, propagation delay τ_π becomes larger for the same L_c value.

Fig. 6 shows the relation between rise time t_r and the summed inductance value after passing through some discontinuities with and/or without matching capacitors. As lumped inductance values become larger, the rise times become abruptly larger, which are somewhat improved by the matching capacitors. The degradation in the rise time after passing through, for example, three 50-pH inductive discontinuities, is smaller than that after passing through one 150-pH inductance discontinuity, because of cutoff frequency difference for the two cases.

Fig. 7 shows the relation between lumped inductance L_c

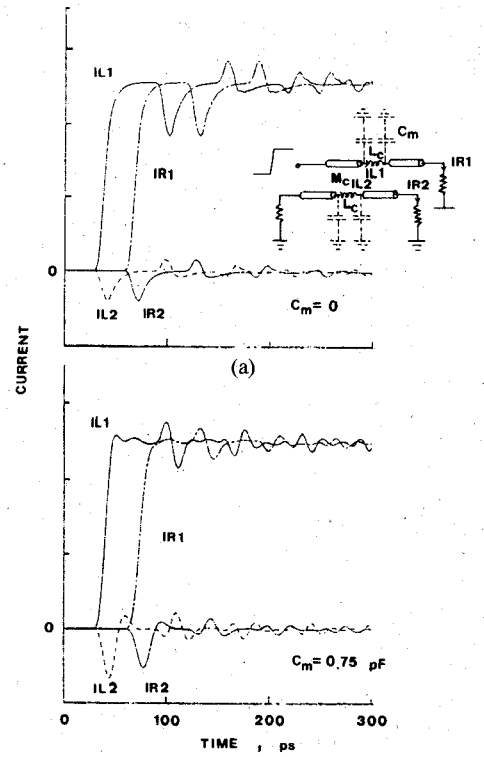

Fig. 8. Circuit configuration, including mutual inductance between other signal line and circuit current responses. (a) Without matching capacitors. (b) With matching capacitors.

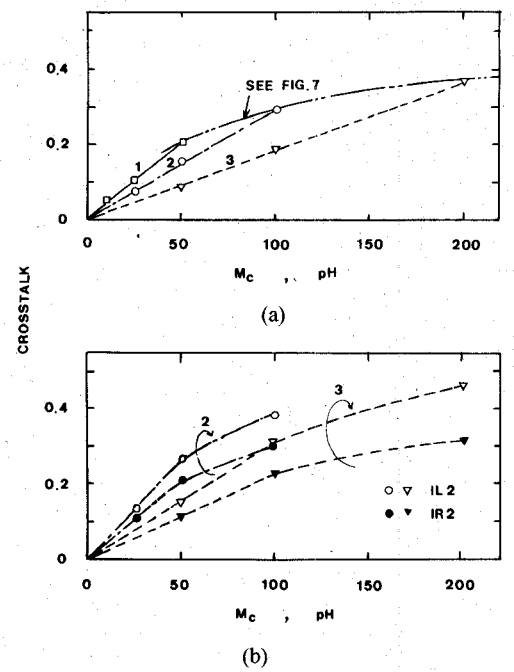

Fig. 9. Relation between crosstalk and mutual inductance. Line 1: $L_c = 50$ pH. Line 2: $L_c = 100$ pH. Line 3: $L_c = 200$ pH. (a) and (b) show the cases without and/or with matching capacitors, respectively.

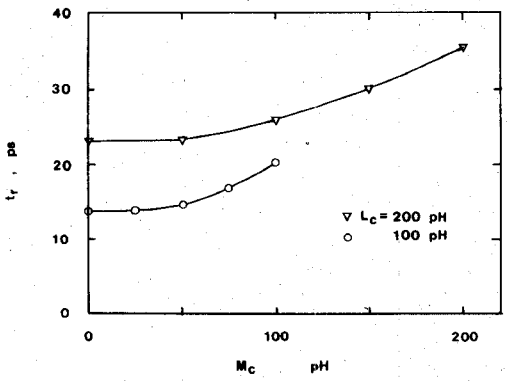

Fig. 10. Relation between signal rise time t_r and mutual inductance M_c without matching capacitors.

and absolute current reflection coefficient r_I at the discontinuity. Above about 200 pH, the coefficient exhibits a saturation tendency. The dashed line represents calculated values for the case where the ladder circuit, made up of the L_cC_0 circuit (characteristic impedance $Z' = \sqrt{L_c/C_0}$) is connected to a stripline whose characteristic impedance is $Z_0 = 10\ \Omega$ (i.e., L_0C_0 ladder circuit), which gives the maximum reflection coefficient. For example, as a typical value, the pulse-like reflection current amplitude for $L_c = 200$ pH is -0.37.

C. Mutual Inductance Influences

In this section, crosstalk problems are mainly discussed, considering mutual inductance between other signal lines at inductive discontinuity.

Fig. 8 (a) and (b) show the simulation results for the circuit shown in the figure, where the self-inductance L_c is 100 pH without and/or with matching capacitors, the mutual inductance M_c is 50 pH, and all the resistors are terminated to characteristic impedance Z_0. For the unmatched case, the reflection amplitude at the inductive discontinuity appears to be decreased to the amplitude for the $(L_c - M_c)$ inductive discontinuity case. For the matched case, due to the mutual inductance, the matching condition at the discontinuity is so deviated that reflection is caused. Moreover, crosstalk to the neighboring signal line is observed and the crosstalk level for the matched case is larger than that for the unmatched case, because of the improved rising performance. Fig. 9 (a) and (b) show the relation between the crosstalk and mutual inductance for cases without and/or with matching capacitors, respectively, including the parameters of self-inductance L_c values. From Fig. 9 (a), it is seen that the crosstalk for the case of larger self-inductance is smaller, provided that the same mutual inductance exists at the discontinuity. It can also be concluded that the maximum crosstalk value for the neighboring signal line is always under the reflection amplitude with the self-inductance $L_c = M_c$. On the other hand, the penalty for matching capacitors C_m is additional crosstalk in the signal traversing the discontinuity to the neighboring signal lines.

Fig. 10 shows the relation between signal rise time t_r and mutual inductance M_c for the case where the self-inductance is not matched using the capacitors. If the mutual inductance M_c is smaller than the self-inductance L_c, degradation in the signal rise time, due to mutual inductance existence at the discontinuity, can be mostly ignored. Fig. 11 shows the relation between signal propagation delays t_{pd}

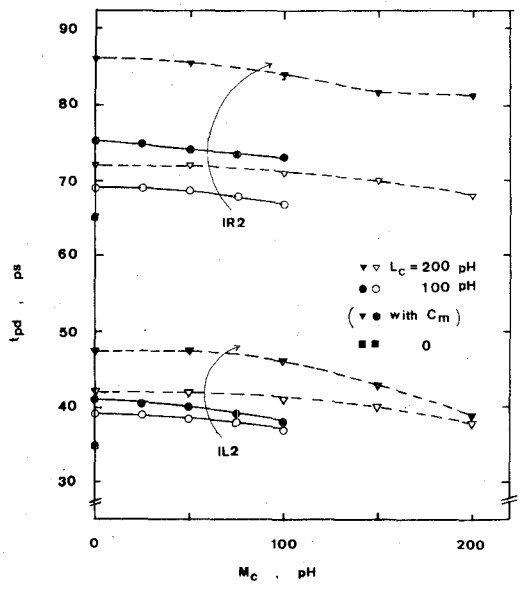

Fig. 11. Relation between propagation delay for the circuit for Fig. 8 (a) and mutual inductance M_c.

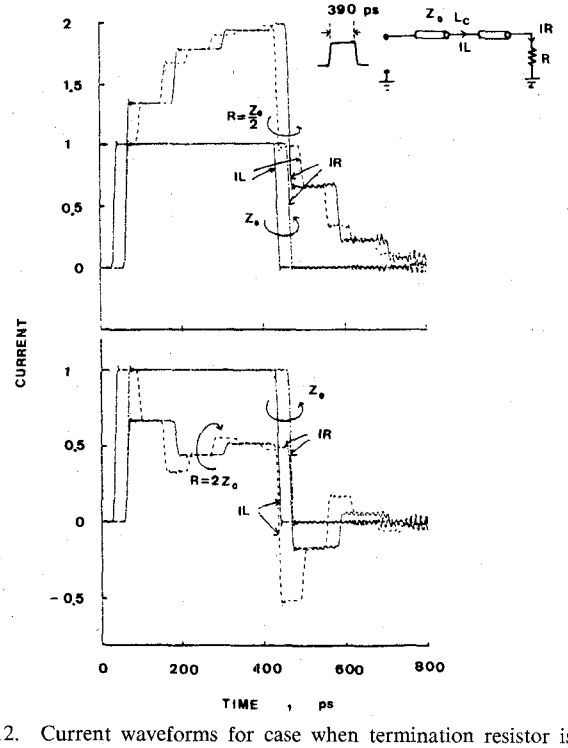

Fig. 12. Current waveforms for case when termination resistor is not matched to characteristic impedance Z_0. Here, lumped inductance L_c is zero.

at the inductive discontinuity and termination resistor and the mutual inductance values. It is also seen that, for this case where the mutual inductance is smaller than the self-inductance, influences on the signal propagation delay can be mostly ignored.

D. Terminated Resistor Influences

For the case where the terminated resistor is different from the characteristic impedance of the line, the circuit responses will be simulated in this section.

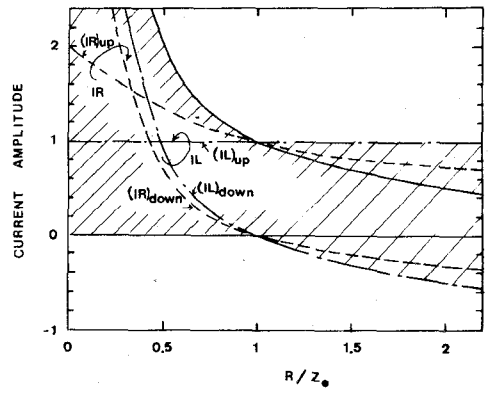

Fig. 13. Relation between transient and stationary current amplitude and normalized termination resistor value R/Z_0 in Fig. 12.

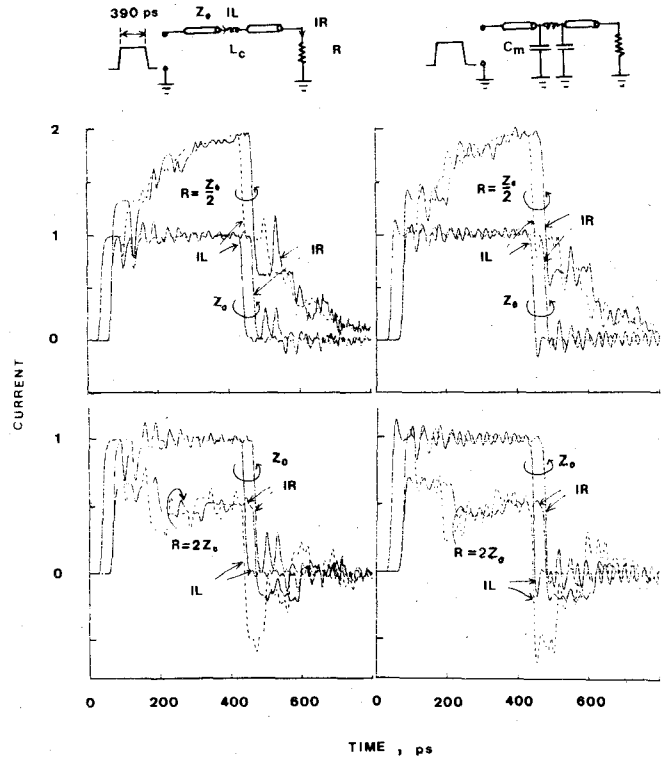

Fig. 14. Current waveforms for case when the termination resistor is not matched to characteristic impedance Z_0. Here, lumped inductance L_c is 100 pH. (a) Without matching capacitors. (b) With matching capacitors.

Fig. 12 shows the simulation results for the circuit configuration in the figure with terminated resistor $R=0.5Z_0$, and $2Z_0$, where the self-inductance L_c at the discontinuity is zero for simplicity. The input voltage signal rise and fall times are 8 ps, respectively, and pulsewidth $\Delta\tau$ is 390 ps, which is sufficiently long compared with the round-trip times between unmatched terminations. At the source end, current reflection coefficient r_I is 1. At the $0.5Z_0$ and $2Z_0$ receive ends, its values are 0.33 and -0.33, respectively. The period for step waveforms in Fig. 12 is $2\tau_{4\ mm}$ and $4\tau_{4\ mm}$ for currents *IL* and *IR*, respectively. Therefore, the step-like current waveforms in Fig. 12 can be reasonably illustrated. Next, the stationary current amplitude and other transient current amplitudes after the first upward

switching and the downward switching, i.e., $(IL)_{up}$, $(IR)_{up}$, $(IL)_{down}$, and $(IR)_{down}$ at the discontinuity with $L_c = 0$ and the resistor element versus normalized termination resistor R/Z_0, are shown in Fig. 13. In Fig. 13, the hatched area indicates the current amplitude variation area for transient and stationary states. Here, it should be noted that, when the R value is larger than the Z_0 value, the transient amplitude after switching to "OFF" exhibits a negative amplitude.

Next, including the finite interconnection inductance L_c without and/or with matching capacitors, the circuit responses are shown in Fig. 14 (a) and (b), where $L_c = 100$ pH. The features of the current waveforms in Fig. 14 are as follows: for the unmatched case, considering current IL, the reflection amplitude due to an inductive discontinuity, apparently exhibits a maximum value for the conditions where the resistor is terminated into the Z_0 value. On the other hand, considering current IR, the terminated resistor value is so much larger than the Z_0 value that the absolute amplitude of reflection becomes smaller. For the case where matching capacitors are added, the amplitude vibrations occur at the stationary value and are not small enough to be ignored, compared with the amplitude distortion due to "bare" inductance reflections.

III. Discussion

In the preceding section, for signal propagation with rise time $t_r = 8$ ps ($T = 10$ ps), some useful relations have been obtained, which are used in designing the Josephson packaging, between the lumped inductance at the discontinuity and propagation delay, the degraded rise time, reflection amplitude, distortions, and crosstalk, including the influences of matching capacitors and the terminated resistor value. Here, in general, if the signal rise time t_r (ps) used is different from 8 ps, its effect is accounted for by multiplying the lumped inductance values by the factor $a = t_r/8$ and replacing L_c (or M_c) with aL_c. The reasons for these actions can be simply determined from the frequency domain considerations.

The Josephson circuits are operated in the latching mode with both polarity possibilities so that the amplitude distortions at the stationary state amplitude can cause no error (which is different from the situation with semiconductor circuits). But degraded signal rise and fall performance due to the lumped inductance, matching capacitors, and terminated resistor causes large adverse influences on normal switching operations (in particular, for the latching mode), from the standpoint of designing precise signal delay and output pulsewidth. On the other hand, matching capacitors, which are used in order to eliminate signal reflections at the inductive discontinuity, are effective from the standpoint of improving signal rise and fall performances. However, the penalty is an additional delay and relatively large amplitude distortions or vibrations at the stationary amplitude, which may become serious problems for achieving high-performance equipment.

In order to reduce amplitude distortions when transmitting ultrafast signals in Josephson technology, it is important not only to reduce interconnection inductance values, but also to realize uniform transmission superconducting lines and well-matched termination resistors. From the viewpoint of designing accurate timing, i.e., signal propagation delay and sharp rising time, accurate theoretical and experimental evaluations of the lumped inductance, which appears at each discontinuity, are important.

In this paper, superconducting contacts at each interconnection discontinuity are assumed for simplicity. However, the evaluation of allowable finite resistance at the discontinuity may become necessary, which is a future work considering the performance of the actual equipment.

IV. Conclusion

The lumped inductance influences of superconducting circuit interconnections on ultrafast switching (~10 ps) signal propagation characteristics, such as signal propagation delay, degraded switching time, amplitude distortions and crosstalk, were quantitatively evaluated for the first time by using the LNAP computer simulation, including the influences of matching capacitors and terminated resistor values.

Acknowledgment

The authors wish to thank Dr. K. Noda, Dr. Y. Kuroyanagi, and Dr. H. Katsuraki for their guidance and encouragement. They also thank H. Yamada for his useful suggestions concerning the LNAP program and K. Aoki and Y. Tazoh for their valuable comments on this study.

References

1) W. Anacker, "Computing at 4 degrees Kelvin," *IEEE Spectrum*, pp. 26–37, May 1979.
2) T. W. Gheewala, "Design of 2.5-micrometer Josephson current injection logic (CIL)," *IBM J. Res. Develop.*, vol. 24, pp. 130–142, Mar. 1980.
3) A. V. Brown, "An overview of Josephson packaging," *IBM J. Res. Devel.*, vol. 24, pp. 167–171, Mar. 1980.
4) H. C. Jones and D. J. Herrel, "The characteristics of chip-to-chip signal propagation in a package suitable for superconducting circuits," *IBM J. Res. Devel.*, vol. 24, pp. 172–177, Mar. 1980.
5) S. K. Lahiri, P. Geledermans, G. Kolb, J. Sokolowski, and M. J. Palmer, "Pluggable connectors for Josephson device packaging," in *Proc. Elec. Chemical Society Conf.* (Abstract), May 1980, pp. 216–217.
6) S. M. Faris, "Generation and measurement of ultrashort current pulses with Josephson devices," *Appl. Phys. Lett.*, vol. 36, no. 12, pp. 1005–1007, June 1980.
7) D. B. Tuckerman, "A Josephson ultrahigh-resolution sampling system," *Appl. Phys. Lett.* vol. 36, no. 12, pp. 1008–1010, June 1980.
8) *Large-scale Network Analysis Program (LNAP)*. Nippon Telegraph and Telephone Public Corporation, Manual no. DEMOS-E 7021.

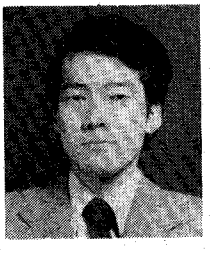

Jiro Temmyo was born in Tokyo, Japan, on January 31, 1949. He received the B.S., M.S., and Ph.D. degrees in electrical engineering from Waseda University, Tokyo, Japan, in 1971, 1973, and 1979, respectively.

In 1973 he joined the Musashino Electrical Communication Laboratory, Nippon Telegraph and Telephone Public Corporation, Tokyo, Japan, where he has been engaged in research and development of surface acoustic wave devices for communications applications. His current research

interests include Josephson computer technology.

Dr. Temmyo is a member of the Institute of Electronics and Communication Engineers of Japan, and in March 1979 he received their Young Engineer Award.

✤

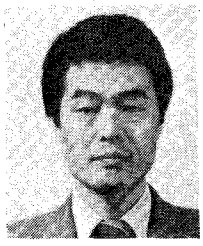

Haruo Yoshikiyo was born in Tokyo, Japan, on November 5, 1941. He received the B.S. degree in electronic engineering from the University of Electro-Communications, Tokyo in 1965 and the M.S. and D.E. degrees from Osaka University, Osaka, Japan in 1967 and 1980, respectively.

In 1967 he joined the Musashino Electrical Communication Laboratory, Nippon Telegraph and Telephone Public Corporation, Tokyo, and worked on optical beam waveguides and optical fiber transmission techniques until 1974. From 1975 to 1979, he studied superconducting transmission cables for communication systems using superconducting coaxial lines. Since 1980, he has been involved with a research group on the Josephson computer technology.

Dr. Yoshikiyo is a member of the Institute of Electronics and Communication Engineers of Japan, and the Cryogenic Association of Japan.

A 26-GHz Band Integrated Circuit of a Double-Balanced Mixer and Circulators

HIROYO OGAWA, MASAMI AKAIKE, MEMBER, IEEE, MASAYOSHI AIKAWA, MEMBER, IEEE, TOSHIROH KARAKI, AND JUNJI WATANABE

Abstract—**Integration of a double-balanced mixer and ferrite-disk type circulators have been successfully achieved in the 26-GHz band. The total single-sideband noise figure of the integrated circuit, composed of a mixer and two circulators, is 8.5 dB, including the noise contribution from an IF amplifier. The double-balanced mixer is composed of microstrip lines, slot lines, coupled slot lines, coplanar lines, Au wires, and four beam lead Schottky-barrier diodes. The minimum conversion loss of the mixer is 5.3 dB at a signal frequency of 25.4 GHz. Isolation between RF and LO ports is greater than 30 dB. The ferrite-disk type circulator is produced by a newly developed precise machining technique. The minimum insertion loss of the circulator is 0.45 dB, and the isolation is greater than 20 dB. The integrated circuit with the ferrite-disk type circulators will be extended to the millimeter-wave band.**

I. INTRODUCTION

RECENTLY, microwave integrated circuits (MIC) have been used to produce various circuits, i.e., oscillators [1], mixers [2], [3], modulators [4], [5], and circulators [6]–[11]. Moreover, MIC transmitters and receivers can be fabricated by combinations of these circuits [12], [13].

Manuscript received April 15, 1981; revised August 19, 1981.

H. Ogawa, M. Akaike, and M. Aikawa are with the Yokosuka Electrical Communications Laboratory, Nippon Telegraph and Telephone Public Corporation, 1-2356 Take, Yokosuka-shi, 238-03, Japan.

T. Karaki and J. Watanabe are with the Musashino Electrical Communications Laboratory, Nippon Telegraph and Telephone Public Corporation, 9-11, 3 Chome, Midoricho, Musashino-shi, Tokyo, 180, Japan.

MIC balanced mixers have been constructed by combinations of microstrip lines and slot lines at millimeter-wave band [14], [15]. A new structure for the double-balanced mixer, that is suitable for high frequency band, has been produced using combinations of microstrip lines, slot lines and coupled slot lines [16], [17]. However, since the mixer uses two plated through holes in the substrate to connect microstrip lines and slot lines, and since the insertion loss increases and the isolation decreases due to these holes, the realizable frequency of the mixer is still limited to the 20-GHz band.

In this paper, a new configuration of a double-balanced mixer has been proposed for use at high frequency bands. Two gold (Au) wires are used to construct an intermediate-frequency (IF) circuit instead of two cylindrical conductors in the substrate. Thereby the insertion loss and the isolation of the mixer has been improved at frequencies above the 20-GHz band.

MIC circulators take an important part in transmitters and receivers. Circulators are used as isolators, combiners, and input/output terminals for reflection-type amplifiers. MIC circulators are divided into two different forms. One form consists of a ferrite disk embedded into a dielectric substrate (referred to as the "ferrite-disk" type) [7], while the other uses an all-ferrite substrate [8]. Generally, most microwave integrated circuits are fabricated on a dielectric

0018-9480/82/0100-0034$00.75 ©1982 IEEE